



Full Length Article

Uptake of Cu²⁺ and Zn²⁺ from simulated wastewater using muskmelon peel biochar: Isotherm and kinetic studies



Tabrez Alam Khan ^{a,*}, Amer Arif Mukhlif ^a, Equbal Ahmad Khan ^b

^aDepartment of Chemistry, Jamia Millia Islamia, Jamia Nagar, New Delhi 110 025, India

^bDepartment of Chemistry, Al-Falah University, Dhauj, Faridabad 121 004, India

ARTICLE INFO

Article history:

Received 23 November 2016

Received in revised form 16 June 2017

Accepted 16 June 2017

Available online 28 June 2017

Keywords:

Copper(II) and zinc(II)

Muskmelon peel biochar

Langmuir

Pseudo-second order

Exothermic

ABSTRACT

The muskmelon peel, an abundant common food waste material, has been gainfully utilized for the production of biochar. The biosorptive characteristics of muskmelon peel biochar towards copper(II) and zinc(II) from water are investigated. The biochar is characterized by infrared spectroscopy (FT-IR), scanning electron microscopy (SEM) and energy dispersive X-ray (EDX) studies. The various process parameters for the removal of copper(II) and zinc(II) using biochar are optimized. The maximum biosorption of Cu(II) and Zn(II) is attained at pH 7. Maximum Langmuir adsorption capacity (q_m) are 78.74 for copper(II) and 72.99 mg/g for zinc(II) at 303 K. Langmuir isotherm is found to best fit the equilibrium data indicating homogeneous adsorption of metal ions onto the biochar surface. The pseudo-second order kinetic model describes the data best indicating adsorption of one molecule of metal ions onto two surface sites. Thermodynamic parameters suggest the adsorption process to be spontaneous and exothermic. Both liquid-film and intra-particle diffusions control the overall kinetics of the adsorption process. Biochar proved to be an inexpensive and efficient adsorbent for the removal of titled metals from liquid phase.

© 2017 Mansoura University. Production and hosting by Elsevier B.V. This is an open access article under the CC BY-NC-ND license (<http://creativecommons.org/licenses/by-nc-nd/4.0/>).

Introduction

The growing industrialization has resulted in an increased influx of industrial effluents containing heavy metals into the aqueous streams. Electroplating and metal surface treatment processes produce large quantity of wastewater containing heavy metals, which include copper(II) and zinc(II). The presence of copper(II) and zinc(II) in aquatic environment, even at low concentrations, is potentially harmful to human health. Copper(II), beyond the maximum concentration limit (0.25 mg/L) can cause liver damage, Wilson disease, insomnia, and depression, while a person exposed to zinc(II) (exposure limit, 0.80 mg/L) is likely to suffer from neurological disorders, lethargy, and thirst. Considering the toxicity and harmful effects of these metals, it is essential to pre-treat metals bearing wastewater before discharging into aquatic system.

Several techniques available for heavy metals removal from wastewater such as reverse osmosis [1], electrocoagulation [2], ultrafiltration [3], dialysis/electrodialysis [4], and solvent extraction [5] are either costly or less effective due to their own limitations. However, the treatment of aqueous effluents using

adsorption of metals onto low cost adsorbents [6–12] is regarded as an efficient and economical alternative. Biosorption using many agricultural biomass has attracted recent attention because of various functional groups available on the surface of biosorbents for the removal of heavy metals/dyes even at very low concentration from aqueous system [13,14].

In recent past, biochar derived from many agricultural wastes has been used as an effective, efficient, and low cost adsorbent for the removal of heavy metals and organic contaminants from water and soil [15] because of its highly porous structure, large surface area, high functional groups and mineral components [16]. Biochars are mainly applied for enhancing soil fertility and crops productivity, reducing emission of green house gases, waste management and energy production [17,18]. Biochars are usually prepared by the pyrolysis of carbon rich agro-solid waste materials. Various agro-wastes have been used as the precursor for the preparation of biochars and utilized for the removal of heavy metals from water, which include corn straw [19], rice straw [20] straws of peanut, soybean and canola [21] sugar beet tailing [22,23], oak wood and oak bark [24], rice husks, olive pomace, orange waste and compost [25].

The surface properties, yield and adsorption capacity of biochar mainly depend upon the type of precursor (lignocellulosic content) and pyrolytic conditions [26,27]. Slow pyrolysis of biomass at low temperature (400–500 °C) with slow heating rate (0.1–1 °C/s) at

* Corresponding author.

E-mail address: takhan501@yahoo.com (T.A. Khan).

large resident time 5–30 min favors high yield of biochar. In intermediate pyrolysis with pyrolytic temperature (500–650 °C), heating rate (0.1–10 °C/min) and resident time 300–1000 s, 15–25% biochar is obtained. Similarly, the pyrolysis at higher temperature (850–1250 °C), heating rate (10–200 °C/s) and small residence time (1–10 s) generally yields 15–25% of biochar. It has been reported [28] that slow pyrolysis generally results in biochars with surface area of 1.8–56 m²/g, while during fast pyrolysis the biochars usually possess surface area between 7 and 50 m²/g [29].

Muskmelon (*Cucumis melo* L.) fruit belonging to *Cucurbitaceae* family, commonly known as kharbuja in India, is abundantly available during summers. The edible portion of the ripe fruit is consumed while the peel is discarded as a biowaste. The major constituent of muskmelon peel is cellulose, protein and polysaccharides (pectic acid) with –OH and –COOH functional groups, which may bind with metal ions. Recently, the muskmelon peel chemically modified with calcium hydroxide has been studied for the removal of Pb(II) from aqueous solution [30] with adsorption capacity of 167.8 mg/g. However, muskmelon peel has not been utilized as a precursor for production of its biochar.

In this study, various operating conditions in batch process such as biochar dose, contact time, initial Cu(II) and Zn(II) concentration, initial solution pH and temperature are optimized. The biosorption efficiency of muskmelon (*Cucumis melo* L.) peel biochar for copper and zinc from water has been assessed. The isotherm, kinetics and thermodynamics of the biosorption process has been evaluated from the experimental data. The surface properties of adsorbent are examined by FTIR and SEM analysis to evaluate the surface functionality and morphology of the biosorbent.

Experimental

Materials

Muskmelon peel was collected from the fruit juice and shake shop (Jamia Nagar, New Delhi, India). CuSO₄·5H₂O, ZnSO₄·7H₂O, NaOH and HCl was obtained from Merck, India.

Preparation of muskmelon peel biochar

The musk melon peel was washed with distilled water to remove adhering dust particles/impurities, and dried in oven at 333 K. The dried biomass was grinded in a mechanical grinder to a particle size of 1–3 mm. For the preparation of biochar, muskmelon peel (200 g) was pyrolysed at 873 K in a Muffle furnace (Matrix Scientific, India) with heating rate of 278 K/min under inert atmosphere (N₂ gas) for 1 h, and cooled to room temperature. The black solid char was crushed with mortar and pestle, washed with distilled water, sieved to less than 75 µm particle size, and stored in an airtight reagent bottle.

Preparation of adsorbate solution

The stock solution (250 mg/L) of copper sulphate pentahydrate [CuSO₄·5H₂O] and zinc sulphate heptahydrate [ZnSO₄·7H₂O] were prepared by dissolving 0.982 g and 1.099 g of the respective salt in double distilled water (1 L). The required solutions were prepared by diluting the stock solution with double distilled water.

Characterization

The surface morphology and elemental composition of biochar was evaluated by using a Carl Zeiss (Sigma 5.05, Germany) scanning electron microscopy conjugated with BRUKER energy disper-

sive X-ray analyzer (EDX). FTIR spectra (4000–400 cm⁻¹) of the biochar were run on a Perkin-Elmer spectrometer (model BX spectrum, United States).

Batch equilibrium studies

Batch adsorption experiments were carried out in a series of 50 mL erlenmeyer flasks. Each flask was filled with 25 mL metal solution of desired concentration (50 mg/L) and adjusted to the desired pH. A known amount (0.02 g) of biochar was added to each flask and kept in isothermal shaker (303 K) at 200 rpm until equilibrium was reached. The supernatant of reaction mixture was separated by centrifugation. The equilibrium concentration of metal ion was determined by AAS (Perkin Elmer, AAnalyst 200). The equilibrium adsorption capacity (q_e , mg/g) and% removal was determined by Eqs. (1) and (2):

$$q_e = \left(\frac{C - C_e}{m} \times V \right) \quad (1)$$

$$\% \text{ Removal} = \left(\frac{C - C_e}{C} \times 100 \right) \quad (2)$$

where C and C_e is the initial and equilibrium concentration of metal ions solution (mg/L), V is the volume of metal solution (L), and m is the mass of adsorbent (g).

All experiments were carried out in triplicate and average values are reported.

Results and discussion

Characterization of adsorbent

FTIR studies

The FTIR spectral studies were performed to elucidate the active surface functional groups, which may provide binding sites for the metal ions. A strong band observed at 3405 cm⁻¹ in the IR spectrum of the muskmelon peel may be assigned to O–H stretching vibration of inter and intramolecular hydrogen bonded phenols and carboxylic acids. The bands at 2930 and 2850 cm⁻¹ are ascribed to aliphatic C–H of carboxylic acid. The strong bands at 1660 and 1410 cm⁻¹ are ascribed to C=O antisymmetric and symmetric stretching vibration in carboxylate group and C–H in plane bending vibration of lignin. A weak peak at 1540 cm⁻¹ is due to C=C stretching vibration of conjugated aromatic ring of lignin. The peaks at 1250 and 1040 cm⁻¹ may be due to C–OH vibrations of carboxylic acids and alcohol groups of cellulose. The shoulder at 800–400 cm⁻¹ corresponds to C=C–H vibration of benzene ring (Fig. 1a). However, in the biochar, the O–H stretching band, of a decreased intensity, appears at 3400 cm⁻¹, which may be due to cleaving of phenolic groups and dehydration of peel structure. The band observed at 2930 cm⁻¹ in the muskmelon peel shifts to 2920 cm⁻¹, whereas the new weak peaks at 1733 and 1573 cm⁻¹ may be attributed to the formation of carbonate and/or carbonate-carboxyl group during pyrolysis. The broad shoulder at 1170 cm⁻¹ is observed due to the rupture of cellulosic/hemicellulosic groups (Fig. 1b). In the spectra of Cu(II)- and Zn(II)-loaded biochar the O–H stretching band at 3400 cm⁻¹ is shifted to 3440 and 3436 cm⁻¹, while the peak at 1170 cm⁻¹ disappears. Similarly, the peak at 1573 cm⁻¹ is observed at 1600 and 1585 cm⁻¹ after the adsorption of Cu(II) and Zn(II), respectively. The new peaks at 1400 (1390) and 1038 (1050) cm⁻¹ suggest an appreciable interaction of the surface functional groups with Zn(Cu) metal ions (Fig. 1c) and (d).

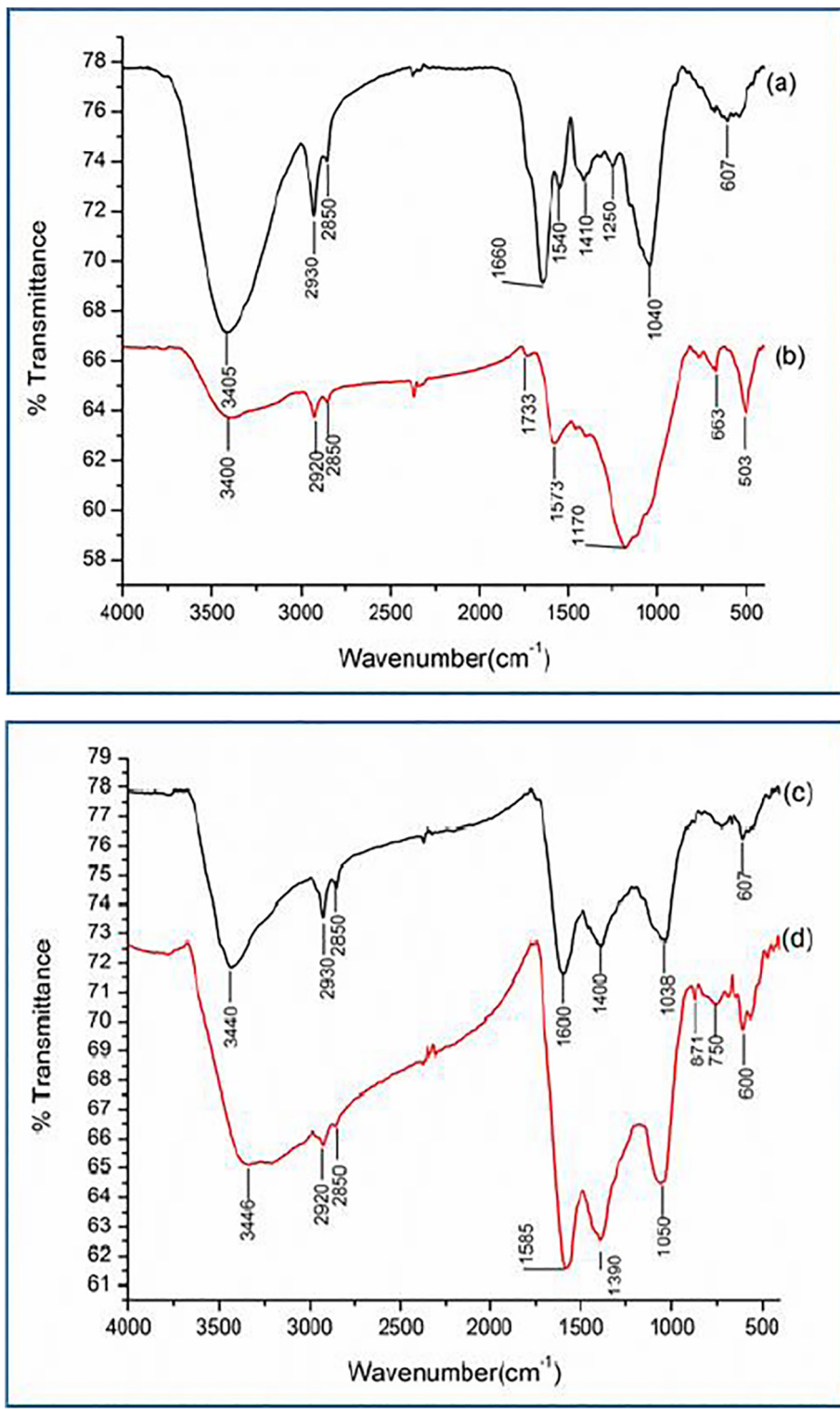


Fig. 1. FTIR spectra of raw muskmelon peel (a), biochar (b), Cu loaded biochar (c), and Zn loaded biochar (d).

SEM and EDX studies

The SEM images (mag. 20,00 KX and 50,00 KX) of raw muskmelon peel exhibit homogeneous and smooth surface with porous structures (Fig. 2a and b). The images of biochar, however, display heterogeneous surface with enlarged porous structures (Fig. 2c and d). The SEM micrographs of metal loaded biochar, however, show that the surface is covered with copper and zinc molecules (Fig. 2e to 2h). The EDS spectra of biochar and metal loaded biochar is shown in Fig. 3. The main constituents of musk-

melon biochar (wt%) are: C (59.28) and O (31.46) with traces of Mg (1.83), P (1.92), K (1.68), and Ca (3.84) (Fig. 3a). After biochar formation, the element wt% are: C (56.43) and O (41.77), Mg (0.40), K (0.79), and Ca (3.84). The P element disappears probably due to heat treatment resulting in the formation of surface voids. In the EDX analyses, after copper and zinc adsorption, new peaks of Cu (1.63 wt%) and Zn (9.50) appear, which indicates the adsorption of these metals on the surface of the biochar (Table 1).

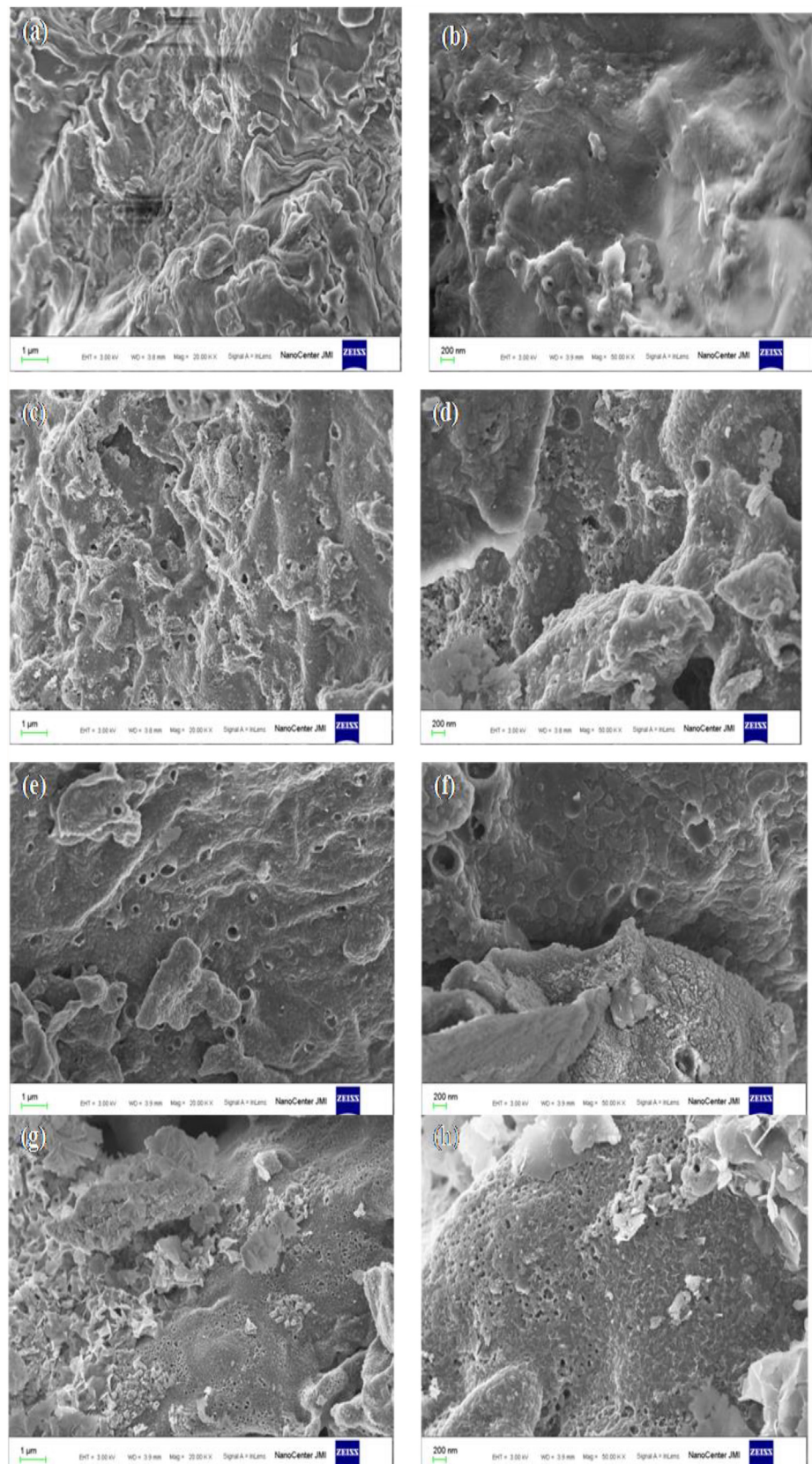


Fig. 2. SEM images at different magnifications of raw muskmelon peel (a,b), biochar (c,d), Cu loaded biochar (e,f), and Zn-loaded biochar (g,h).

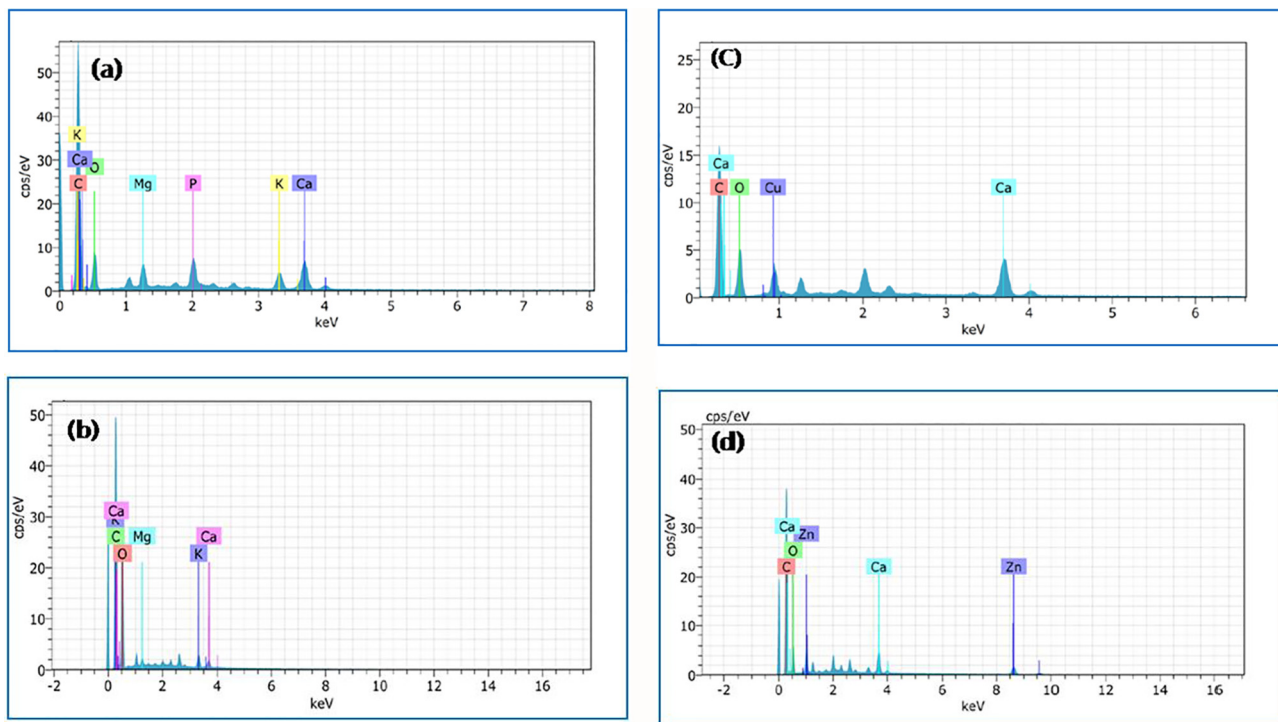


Fig. 3. EDS spectra of raw muskmelon peel (a), biochar (b), Cu-loaded (c), and Zn-loaded (d) biochar.

Table 1
Thermodynamic parameters.

Adsorbate	ΔH° (kJ/mol)	ΔS° (J/mol/K)	$-\Delta G^\circ$ (kJ/mol)		
			303 K	313 K	323 K
Cu(II)	-32.712	-87.19	6.293	5.421	4.549
Zn(II)	-18.039	-43.88	4.743	4.304	3.865

Equilibrium adsorption studies

Effect of contact time

The optimum contact time for the removal of Cu(II) and Zn(II) by biochar was determined by varying the contact time between

10 and 140 min at initial metal concentration (50 mg/L), dose (0.8 g/L), pH (7) and 303 K. It was observed (Fig. 4) that the percent removal of Cu(II) increases from 44.4 to 90.2 and Zn(II) from 35.4 to 83.5 with increasing contact time, attaining equilibrium at 120 min (90.2 for Cu(II) and 83.5 for Zn(II)) (Fig. 4). The initial rapid uptake of metal ions may be ascribed to the presence of large number of vacant sites available for metal ions, and afterwards the remaining free metal ions are difficult to be occupied, because of repulsive forces between the free and adsorbed metal ions.

Effect of initial metal concentrations

Batch experiment is to study the effect of initial metal concentration on the percentage removal of copper(II) and zinc(II) by biochar was carried out at fixed contact time (120 min), dose (0.8 g/L),

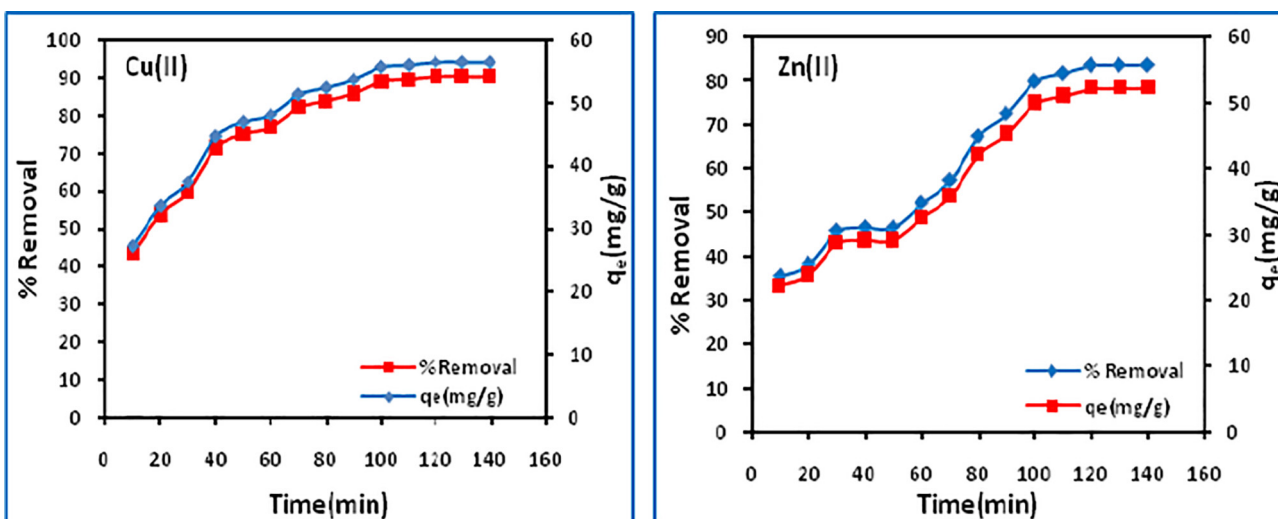


Fig. 4. Effect of contact time on Cu(II) and Zn(II) uptake.

temperature (303 K) and pH (7) but varying the initial concentration from 30 to 60 mg/L. It is found that the adsorption is dependent on initial metal concentrations with percentage uptake of copper(II) and zinc(II) decreasing from 99 to 89.5 and 96.6 to 83.5, respectively, with increasing initial metal concentrations (Fig. 5). However, the adsorption capacity increases from 37.1 to 70.8 mg/g for copper(II) and 36.2 to 71.4 mg/g for zinc(II). The optimum adsorption takes place at 60 mg/L.

Effect of biochar dose

In this study, the biochar dose was varied from 0.2 to 1.2 g/L at optimized contact time (120 min) and initial metal concentration (50 mg/L). The variation in percentage removal of copper(II) and zinc(II) together with biochar adsorption capacity is depicted in (Fig. 6), which indicates that the percent adsorption of copper(II) and zinc(II) increases from 41.3 to 89.2 and 52 to 85.2 with increasing dose (Fig. 6), with maximum percentage removal occurring at 0.8 g/L. This might be attributed to the greater availability of the active sites for adsorption or increase in the surface area at higher amount of the adsorbent dose.

Effect of pH

The effect of pH on the removal of Cu(II) and Zn(II) was evaluated at varying pH (2–9) keeping other parameters constant. The amount of uptake (%) increases from 42.0 to 93.3 and 39.5 to 86.0 for copper and zinc, respectively between pH 2 and 9, due to decrease in competition between H_3O^+ and metal cations (Fig. 7). At pH above pH_{zpc} (6.5), surface attains a negative charge while at pH below pH_{zpc} the surface acquires a positive charge. With increase in the initial solution pH, copper(II) and zinc(II) exist in a variety of species such as $\text{Cu}_2(\text{OH})_2^{2+}$, $\text{Cu}_3(\text{OH})_4^{2+}$, CuOH^+ , $\text{Cu}_2(\text{-OH})_3^+$, $\text{Cu}(\text{OH})_2$ and Zn^{2+} , $\text{Zn}(\text{OH})^+$, $\text{Zn}(\text{OH})_2$ and $\text{Zn}(\text{OH})_3^-$. Below pH 7, copper(II) and zinc(II) exist predominantly as divalent cations and pH > 7, metal cations may precipitate due to formation of hydroxyl species. The maximum adsorption occurs at pH 7.

Effect of temperature and thermodynamic studies

The effect of temperature on the removal of copper(II) and zinc(II) by biochar was studied at 303, 308 and 313 K, and is shown in Fig. 8. The removal of metals (%) decreases with increase in temperature, indicating the adsorption process to be exothermic. The increase in temperature increases the solubility and decreases

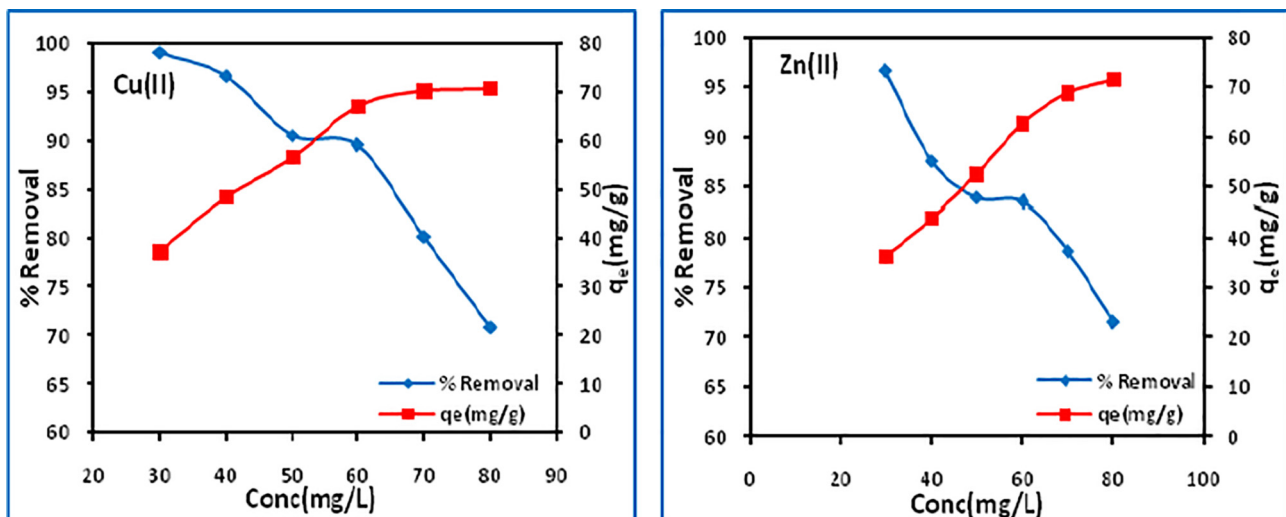


Fig. 5. Effect of initial metal concentration on Cu(II) and Zn(II) uptake.

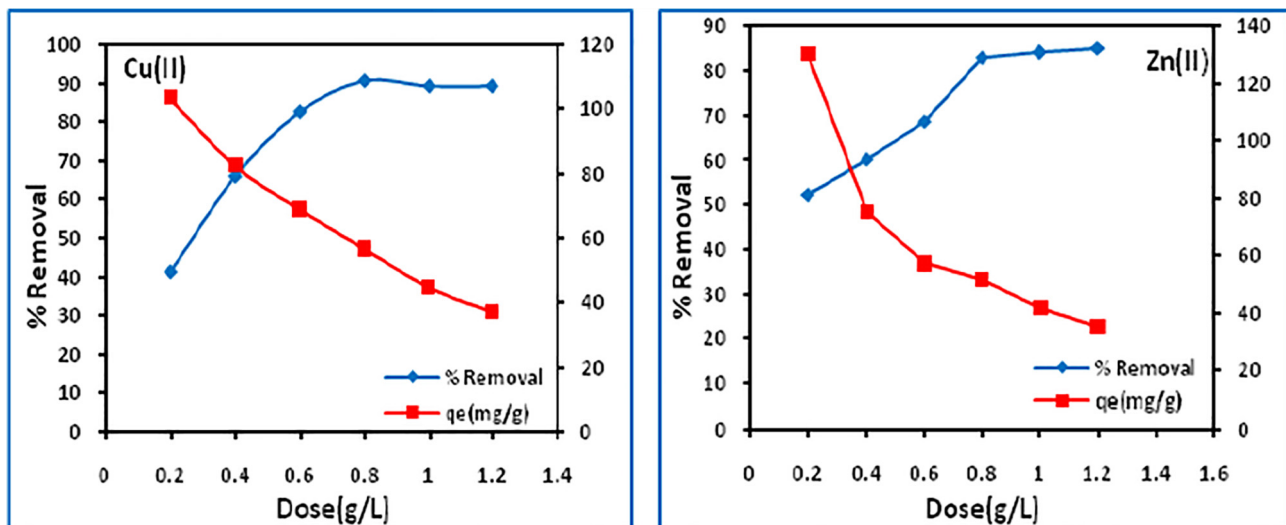


Fig. 6. Effect of biochar dose.

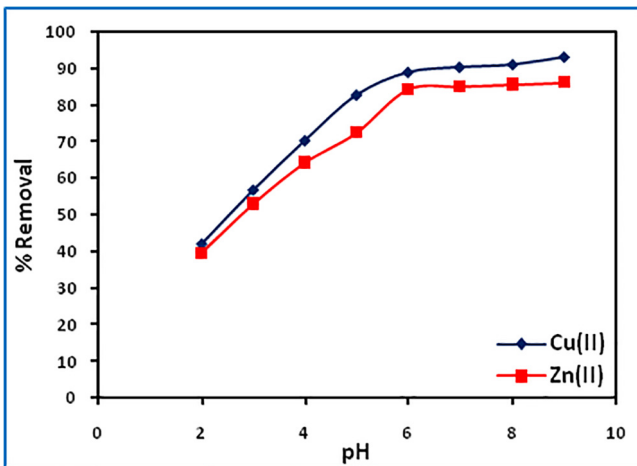


Fig. 7. Effect of initial solution pH.

the chemical potential of the adsorbate, a controlling factor in the adsorption process, thereby resulting in a decrease in adsorption.

To understand the kinetics of adsorption, the energy and entropy considerations are important. Negative ΔG° indicates the spontaneity of the adsorption process. ΔH° is used to identify the exothermic or endothermic nature of adsorption. A positive value of ΔS° indicates increased randomness of adsorbate molecules on the solid surface than in the solution.

The change in enthalpy (ΔH°) and entropy (ΔS°) were determined from the slope and intercept, respectively of the vant Hoff's plot of $\log(q_e/C_e)$ vs $1/T(K)$ (Fig. 9). The free energy change (ΔG°) was calculated using the Gibb's equation (Eqs. (3) and (4)).

$$\log\left(\frac{q_e}{C_e}\right) = \frac{\Delta S^\circ}{2.303R} - \frac{\Delta H^\circ}{2.303RT} \quad (3)$$

$$\Delta G^\circ = \Delta H^\circ - T\Delta S^\circ \quad (4)$$

The negative ΔH° values indicate the exothermic nature of the adsorption of copper(II) and zinc(II) onto biochar. The ΔH° values, 32.712 for Cu(II) and 18.039 kJ/mol for Zn(II), are found to be lower than 40 kJ/mol, supporting physisorption [31] (Table 1). The negative ΔS° values suggest the probability of favorable adsorption. The

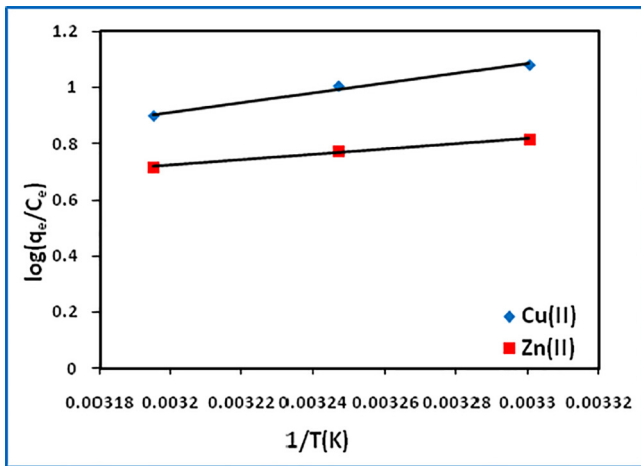


Fig. 9. vant Hoff's plot.

decrease in spontaneity (ΔG° becoming less negative) adsorption process with increase in temperature indicates more feasible adsorption at lower temperature.

Equilibrium studies

Equilibrium studies explain the ratio of the amount of adsorbate adsorbed and that remaining in solution at a constant temperature when equilibrium has been achieved. Langmuir [32], Freundlich [33] and Dubinin-Radushkevich [34] isotherm models were applied to the experimental data to determine the best fit model.

Langmuir isotherm model

If the experimental data fits the Langmuir model it indicates an energetically homogeneous adsorption sites and a uniform coverage of adsorbate molecules onto adsorbent surface without any interaction between adsorbed molecules. The linear form of the Langmuir isotherm model is expressed as follows:

$$\frac{C_e}{q_e} = \frac{1}{bq_m} + \frac{C_e}{q_m} \quad (5)$$

where b is the Langmuir constant related to the energy of adsorption, and q_m is the maximum adsorption capacity (mg/g).

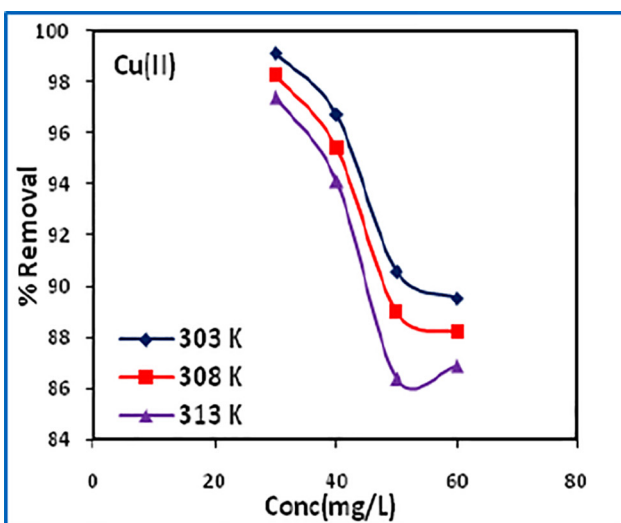
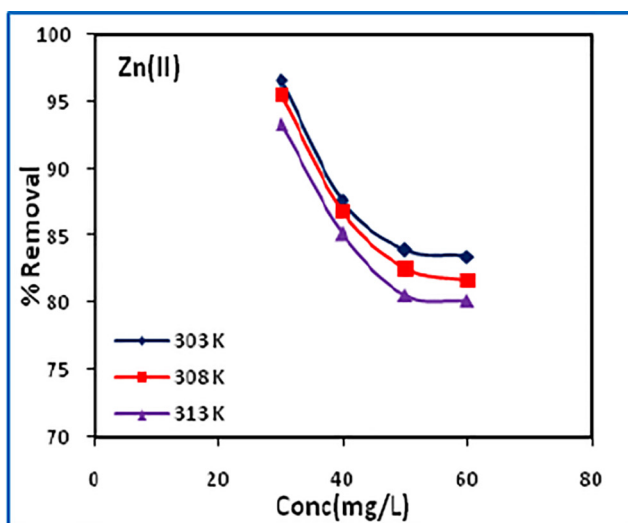


Fig. 8. Effect of temperature.



The monolayer adsorption capacity (q_m) and Langmuir constant (b) representing affinity of adsorbate to adsorbent were calculated from the slope and intercept of the C_e/q_e vs C_e plot (Fig. 10), and are given in Table 2.

The dimensionless separation factor (R_L) [35], can be used to predict the type of adsorption (favorable, linear, unfavorable or irreversible).

$$R_L = \frac{1}{(1 + bC_o)} \quad (6)$$

If $R_L > 1$, the adsorption is unfavorable; if $0 < R_L < 1$, the adsorption is favorable; and if $R_L = 0$, the adsorption is irreversible. The affinity of adsorption of metal ions is in the 0.054–0.075 range for Cu(II) and 0.013–0.015 for Zn(II), which suggests that the adsorption process is highly favorable.

Correlation coefficients (R^2) of all the studied isotherm models are compared to find out the best fit model (Table 2), which indicate that the adsorption data best follows the Langmuir isotherm model. A comparison of q_m values for copper (79.36 mg/g) and zinc (72.99 mg/g) with other reported adsorbents (Table 3) suggests that muskmelon peel biochar is superior to many of these adsorbents. Higher values of b for copper(II) compared to zinc(II) revealed that the biochar has higher affinity towards copper(II).

Freundlich isotherm

This model is based on heterogeneous distribution of adsorption sites on the surface of an adsorbent. The linear form of the Freundlich equation is as follows:

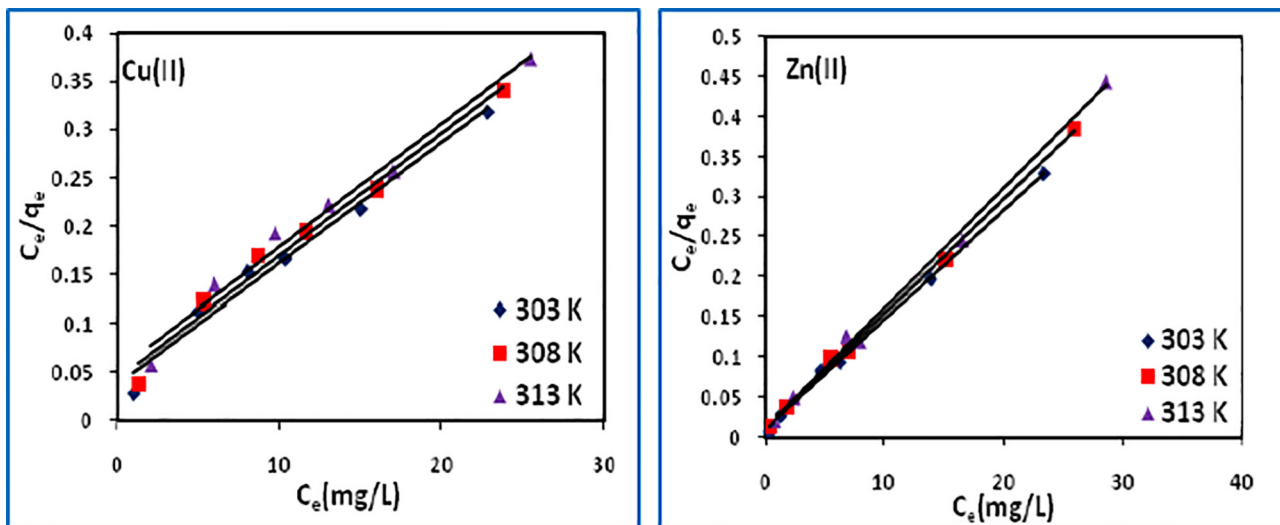


Fig. 10. Langmuir adsorption isotherm plots.

Table 2
Various isotherm parameters.

Isotherm Parameter	Cu(II)			Zn(II)		
	303 K	308 K	313 K	303 K	308 K	313 K
Langmuir	q_m (mg/g)	79.36	78.74	78.74	72.99	69.93
	b (L/mg)	0.349	0.304	0.246	1.505	1.375
	R_L	0.0542	0.0616	0.0751	0.0131	0.0143
	R^2	0.980	0.981	0.982	0.998	0.998
Freundlich	K_f (L/g)	34.03	31.49	27.54	40.04	46.37
	$1/n_f$	0.235	0.252	0.285	0.171	0.167
	R^2	0.919	0.942	0.957	0.884	0.928
D-R	q_D (mg/g)	59.73	60.53	61.33	60.82	62.29
	E (kJ/mol)	1.000	1.000	1.118	2.236	2.500
	R^2	0.897	0.900	0.902	0.804	0.796

Table 3Adsorption capacity (q_m) of reported adsorbents for Cu(II) and Zn(II) uptake.

Cu(II)				Zn(II)			
Adsorbent	pH	q_m (mg/g)	Ref	Adsorbent	pH	q_m (mg/g)	Ref
Wheat shells	5.0	8.26	[36]	Rice husk ash	6.0	5.88	[47]
Arc shell	3–6	17.64	[37]	Bagasse fly ash	6.0	7.03	[48]
Cashew nut shells	5.0	20.0	[38]	Zeolite 4A	6.5	42.82	[49]
Betula sp saw dust	5.5	4.90	[39]	Zeolite 13X	6.5	38.31	[49]
Barly straw	7.0	4.64	[40]	Bentonite	6.5	35.17	[49]
Citric acid modified barly straw	7.0	31.71	[41]	Jute unmodified	5.87	3.55	[50]
Garden grass	6.0	58.34	[41]	Jute dye loaded	5.87	5.95	[50]
Hardwood biochar	5.0	6.79	[19]	Jute oxidized	5.87	8.02	[50]
Corn straw biochar	5.0	12.52	[19]	Vermiculite	5.6	71.89	[51]
Citric acid modified Spent coffee grains	5.0	60.37	[42]	Bentonite	6.0	30.7	[52]
HNO_3 -modified CNTs	5.0	28.49	[43]	Na-enriched bentonite	6.0	57.43	[52]
CNTs/calcium alginate composites	5.0	84.88	[44]	Sulphured orange peel	5.0	80	[53]
Muskmelon peel biochar	7.0	79.36	This study	Muskmelon peel biochar	7.0	72.99	This study
Sulfonated multiwalled carbon nanotubes (sMWCNTs)	5.0	43.16	[45]	KCl modified orange peel	5–5.5	45.29	[53]
Single walled carbon nanotubes (SWCNTs)	5.0	24.29	[46]	Nano-porous activated neem bark	–	11.9	[54]

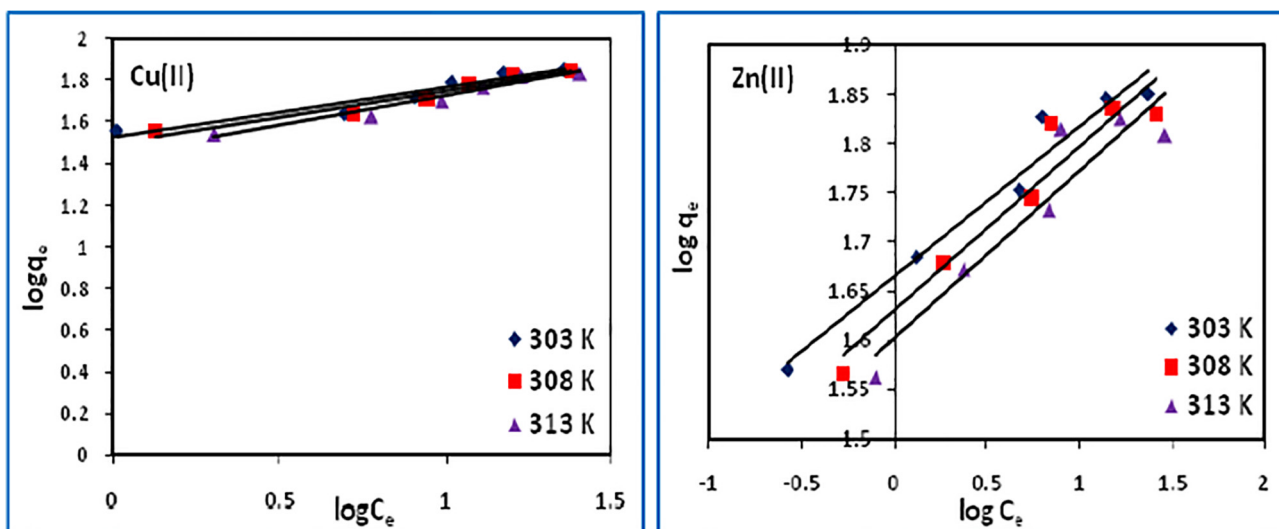


Fig. 11. Freundlich adsorption isotherm plots.

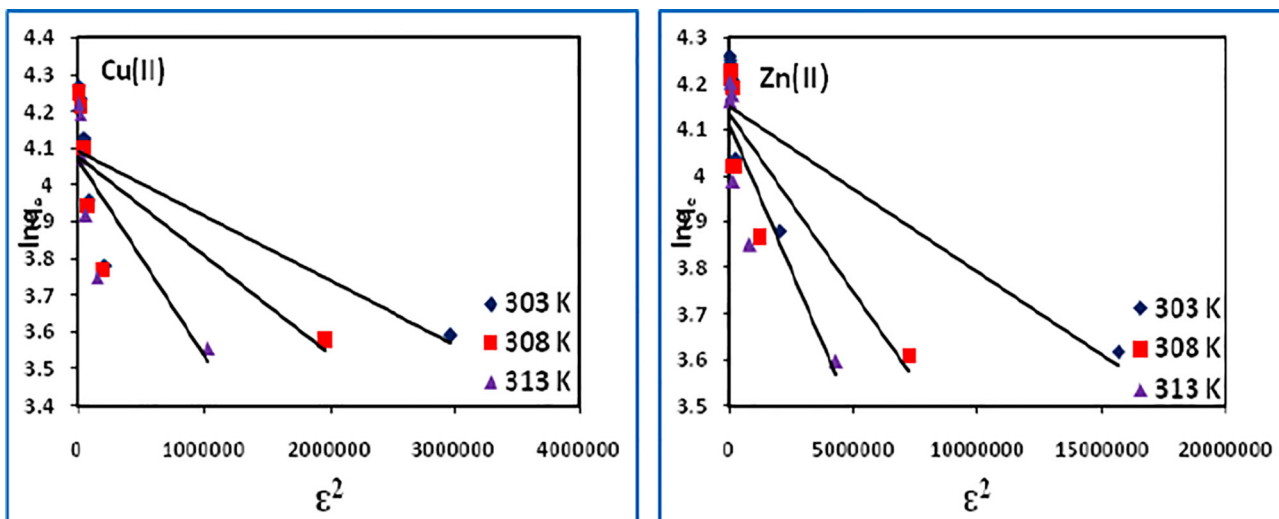


Fig. 12. D-R adsorption isotherm plots.

$$E = \frac{1}{\sqrt{2\beta}} \quad (10)$$

The values of E (1.0–1.12 for Cu(II) and 2.23–3.53 kJ/mol for Zn(II)) are found in the range 0–8 kJ/mol, indicating the adsorption process to be physical in nature. The values of R^2 (0.897–0.902 for Cu(II) and 0.763–0.804 for Zn(II)), however, suggest a poor fit of the model.

Kinetic studies

Pseudo-first order and pseudo-second order

The dynamics of the adsorption was investigated using Lagergren's pseudo-first order [55] and pseudo-second order equations [56]. The pseudo-first order model and pseudo-second order model can be expressed as:

$$\log(q_e - q_t) = \log q_e - \frac{k_1 \cdot t}{2.303} \quad (11)$$

$$\frac{t}{q_t} = \frac{1}{(k_2 q_e^2)} + \frac{t}{q_e} \quad (12)$$

where q_t (mg/g), is the amounts of metal ions adsorbed at time t , k_1 and k_2 is the pseudo-first-order (1/min) and pseudo-second-order rate constant (g/mg/min).

The k_1 and k_2 were calculated from the intercept of the corresponding plots of $\log(q_e - q_t)$ vs t , (Fig. 13) and t/q_t vs t (Fig. 14), and are tabulated in Table 4 along with correlation coefficients, $q_{e(calc)}$ and $q_{e(exp)}$ values. The higher R^2 values and close agreement between $q_{e(calc)}$ and $q_{e(exp)}$ values for the pseudo-second order rate equation suggest the suitability of the model indicating adsorption of one dye molecule onto two surface sites.

Liquid-film and intra-particle diffusions

The adsorption rate constant for liquid-film diffusion, K_{fd} (1/min) and the intra-particle diffusion rate constant, k_i (mg/g min $^{1/2}$) were calculated from the slope of the corresponding plots of $\ln(1 - F)$ vs t [57] and q_t vs $t^{0.5}$ [58] as:

$$-\ln \left(1 - \frac{q_t}{q_e} \right) = k_{fd} \cdot t \quad (13)$$

$$q_t = k_i \cdot t^{0.5} + C_i \quad (14)$$

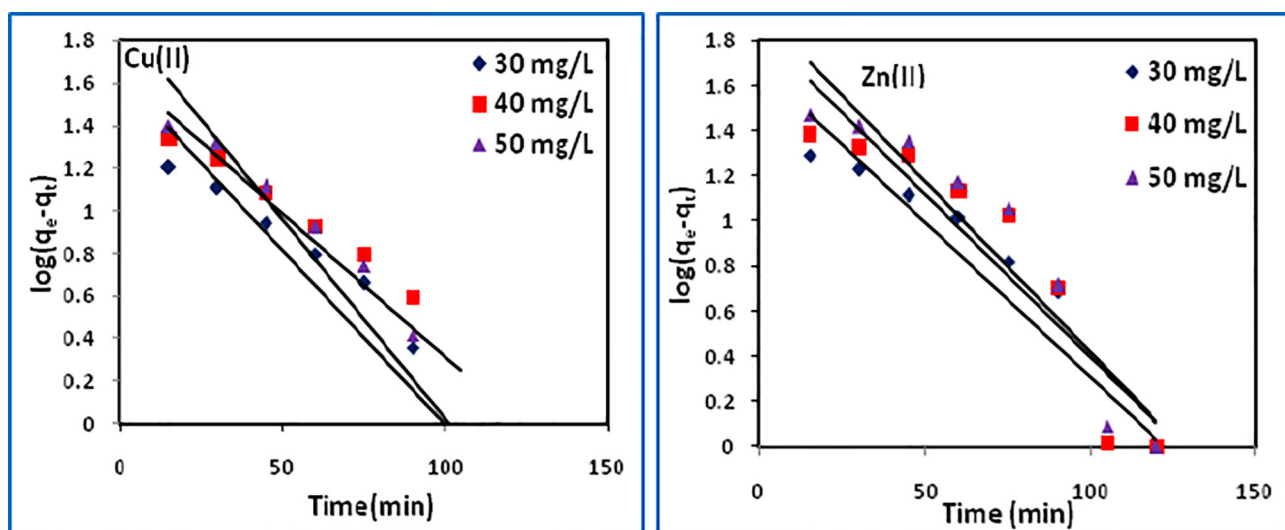


Fig. 13. Pseudo-first order kinetic plots.

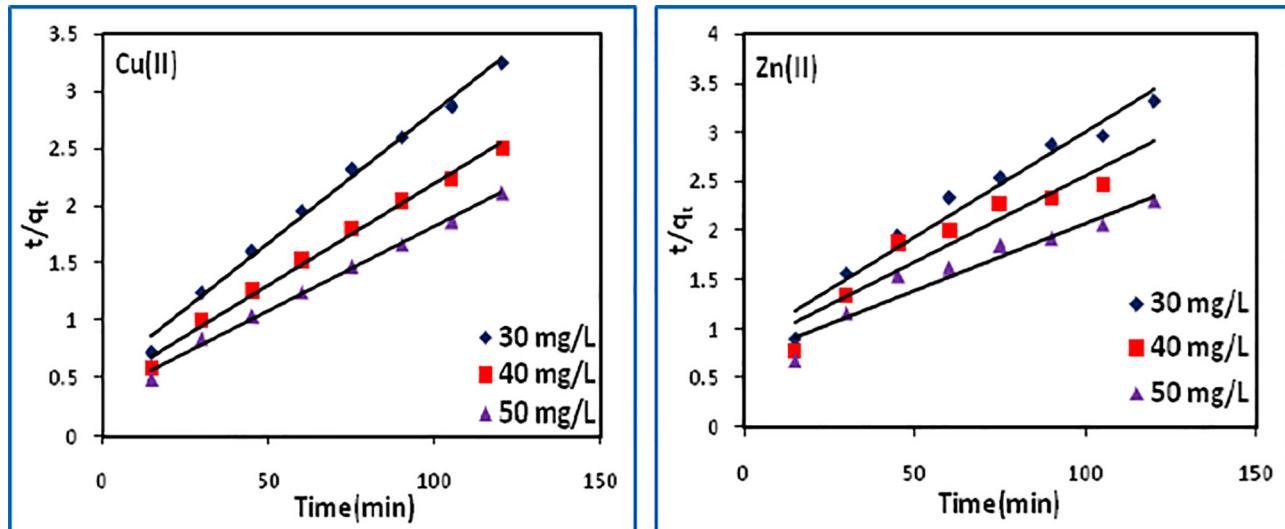


Fig. 14. Pseudo-second order kinetic plots.

Table 4

Pseudo-first order and pseudo-second order model parameters.

Adsorbate	Conc (mg/L)	Pseudo-first order			$q_{e(\text{exp})}$ (mg/g)	Pseudo-second order		
		$k_1 \times 10^{-2}$ (1/min)	$q_{e(\text{cal})}$ (mg/g)	R^2		$k_2 \times 10^{-3}$ (g/mg/min)	$q_{e(\text{cal})}$ (mg/g)	R^2
Cu(II)	40	3.754	43.06	0.839	48.36	1.060	43.10	0.992
	50	3.086	45.77	0.899	56.60	0.750	56.49	0.992
	60	4.306	79.14	0.861	67.13	0.660	67.11	0.994
Zn(II)	40	3.155	47.97	0.860	43.82	0.529	46.73	0.993
	50	3.316	68.12	0.866	52.45	0.393	56.50	0.899
	60	3.477	85.23	0.893	62.08	0.263	72.99	0.930

where k_{fd} (1/min) is the film-diffusion rate constant, and F is the fractional attainment of equilibrium ($F = q_t/q_e$) at time t , k_i (mg/g min^{0.5}) is intra-particle diffusion rate constant, C_i is a constant (mg/g) which gives an idea about the thickness of the boundary layer on the adsorbent surface.

The liquid-film diffusion plots are linear (Fig. 15), but do not pass through the origin so it may not be the only controlling factor in determining the kinetics of the process. The intra-particle diffu-

sion plots (Fig. 16) have the three steps of adsorption, i) an initial curved portion attributed to the bulk diffusion ii), a linear portion to the intra-particle diffusion, and iii) a plateau due to the equilibrium. The magnitudes of k_{fd} , k_i and the corresponding regression coefficients are listed in Table 5. The k_i values indicate substantial diffusion of copper(II) and zinc(II). It may be inferred that both the liquid-film and intra-particle diffusion are be controlling the adsorption kinetics.

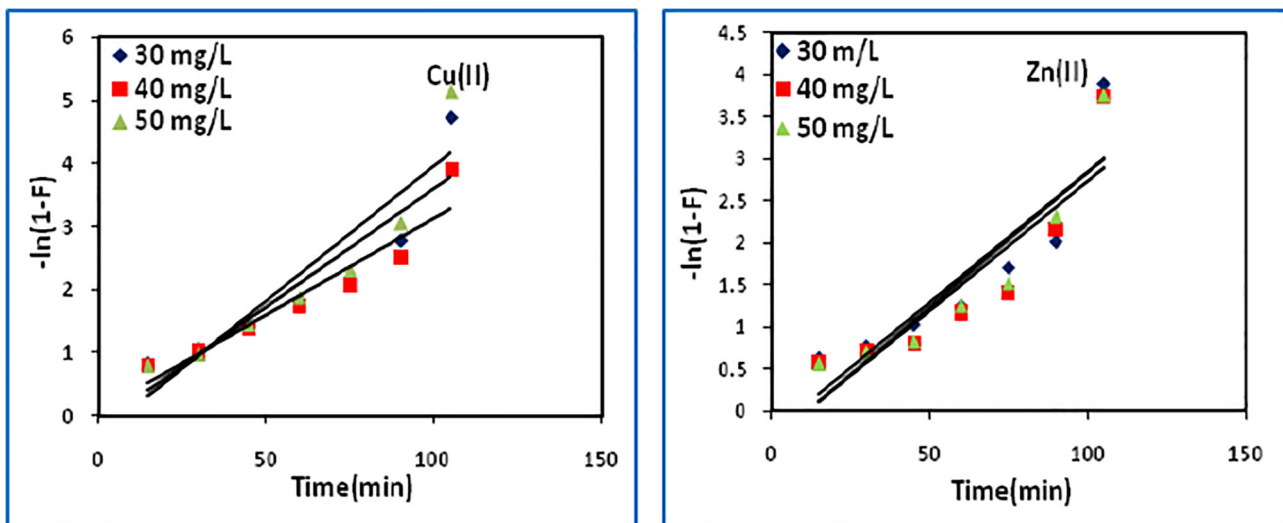


Fig. 15. Liquid-film diffusion plots.

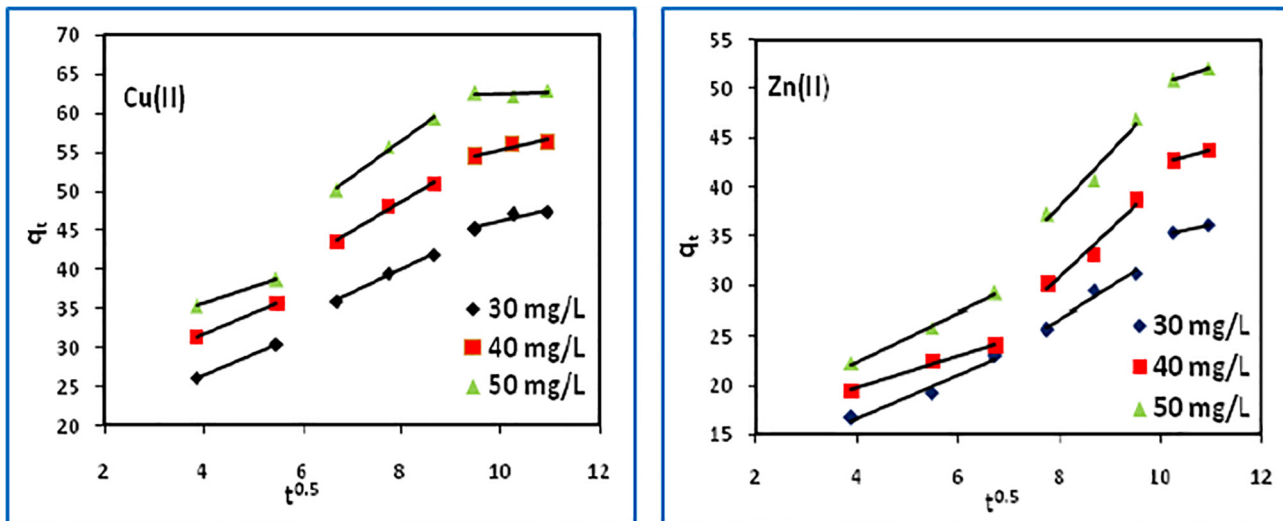


Fig. 16. Intra-particle diffusion plots.

Table 5

Liquid-film and intra-particle diffusion model parameters.

Adsorbate	Conc (mg/L)	Liquid-film diffusion		Intra-particle diffusion	
		k_D	R^2	k_i	R^2
Cu(II)	40	0.0430	0.861	3.853	0.976
	50	0.0375	0.838	3.215	0.992
	60	0.0309	0.899	2.386	0.992
Zn(II)	40	0.0309	0.798	4.656	0.971
	50	0.0308	0.799	3.767	0.956
	60	0.0321	0.840	2.934	0.983

Conclusions

The process parameters for removal of copper and zinc using biochar are optimized. Maximum Langmuir adsorption capacity (q_m) are 78.74 for copper(II) and 72.99 mg/g for zinc(II) at 303 K. The values of R_L between zero and unity supported favorable adsorption. Langmuir isotherm is found to best fit the equilibrium data indicating homogeneous adsorption onto the biochar surface. The pseudo-second order kinetic model describes the data best indicating adsorption of one molecule of metal ions onto two surface sites. Thermodynamic parameters suggest the adsorption process to be spontaneous and exothermic. Both liquid-film and intra-particle diffusions control the overall kinetics of the adsorption process. Biochar proved to be an inexpensive and efficient adsorbent for the removal of titled metals from aqueous solution.

References

- [1] Kurniawan TA, Chan GY, Lo WH, Babel S. Physico-chemical treatment techniques for wastewater laden with heavy metals. *Chem Eng J* 2006;118(1):83–98.
- [2] Ali I, Khan TA, Asim M. Removal of arsenate from groundwater by electrocoagulation method. *Environ Sci Poll Res* 2012;19(5):1668–76.
- [3] Ghosh G, Bhattacharya PK. Hexavalent chromium ion removal through micellar enhanced ultrafiltration. *Chem Eng J* 2006;119(1):45–53.
- [4] Khattab IA, Shafei MF, Shaaban NA, Hussein HS, El-Rehim SA. Electrochemical removal of copper ions from dilute solutions using packed bed electrode. Part II. *Egypt J Petrol* 2013;22(1):205–10.
- [5] Černá M. Use of solvent extraction for the removal of heavy metals from liquid wastes. *Environ Monit Assess* 1995;34(2):151–62.
- [6] Khan TA, Nazir M, Khan EA. Magnetically modified multiwalled carbon nanotubes for the adsorption of bismarck brown R and Cd(II) from aqueous solution: batch and column studies. *Desalination Water Treat* 2015;11:19374–90.
- [7] Khan TA, Nazir M, Khan EA, Riaz U. Multiwalled carbon nanotube-polyurethane (MWCNT/PU) composite adsorbent for safranin T and Pb(II) removal from aqueous solution: batch and fixed-bed studies. *J Mol Liq* 2015;212:467–79.
- [8] Khan TA, Singh VV. Removal of cadmium(II), lead(II), and chromium(VI) ions from aqueous solution using clay. *Toxicol Environ Chem* 2010;92(8):1435–46.
- [9] Saleh TA, Gupta VK. Column with CNT/magnesium oxide composite for lead(II) removal from water. *Environ Sci Poll Res* 2012;19(4):1224–8.
- [10] Gupta VK, Agarwal S, Saleh TA. Synthesis and characterization of alumina-coated carbon nanotubes and their application for lead removal. *J Hazard Mater* 2011;185(1):17–23.
- [11] Gupta VK, Nayak A. Cadmium removal and recovery from aqueous solutions by novel adsorbents prepared from orange peel and Fe_2O_3 nanoparticles. *Chem Eng J* 2012;180:81–90.
- [12] Khan TA, Mukhlif AA, Khan EA, Sharma DK. Isotherm and kinetics modeling of Pb(II) and Cd(II) adsorptive uptake from aqueous solution by chemically modified green algal biomass. *Model Earth Syst Environ* 2016;2:117.
- [13] Gupta VK, Srivastava SK, Mohan D, Sharma S. Design parameters for fixed bed reactors of activated carbon developed from fertilizer waste for the removal of some heavy metal ions. *Waste Manag* 1998;17(8):517–22.
- [14] Mohammadi N, Khani H, Gupta VK, Amereh E, Agarwal S. Adsorption process of methyl orange dye onto mesoporous carbon material-kinetic and thermodynamic studies. *J Colloid Interface Sci* 2011;362(2):457–62.
- [15] Wang G, Li A, Li M. Sorption of nickel ions from aqueous solutions using activated carbon derived from walnut shell waste. *Desalination Water Treatment* 2010;16(1–3):282–9.
- [16] Lonappan L, Rouissi T, Das RK, Brar SK, Ramirez AA, Verma M, Surampalli RY, Valero JR. Adsorption of methylene blue on biochar microparticles derived from different waste materials. *Waste Manag* 2016;49:537–44.
- [17] Yang K, Yang J, Jiang Y, Wu W, Lin D. Correlations and adsorption mechanisms of aromatic compounds on a high heat temperature treated bamboo biochar. *Environ Poll* 2016;210:57–64.
- [18] Lehmann J. A handful of carbon. *Nature* 2007;447(7141):143–4.
- [19] Chen X, Chen G, Chen L, Chen Y, Lehmann J, McBride MB, Hay AG. Adsorption of copper and zinc by biochars produced from pyrolysis of hardwood and corn straw in aqueous solution. *Bioresour Technol* 2011;102(19):8877–84.
- [20] Han X, Liang CF, Li TQ, Wang K, Huang HG, Yang XE. Simultaneous removal of cadmium and sulfamethoxazole from aqueous solution by rice straw biochar. *J Zhejiang Univ Sci B* 2013;14(7):640–9.
- [21] Tong XJ, Li JY, Yuan JH, Xu RK. Adsorption of Cu(II) by biochars generated from three crop straws. *Chem Eng J* 2011;172(2):828–34.
- [22] Dong X, Ma LQ, Li Y. Characteristics and mechanisms of hexavalent chromium removal by biochar from sugar beet tailing. *J Hazard Mater* 2011;190(1):909–15.
- [23] Yao Y, Gao B, Inyang M, Zimmerman AR, Cao X, Pullammanappallil P, Yang L. Removal of phosphate from aqueous solution by biochar derived from anaerobically digested sugar beet tailings. *J Hazard Mater* 2011;190(1):501–7.
- [24] Mohan D, Kumar H, Sarswat A, Alexandre-Franco M, Pittman CU. Cadmium and lead remediation using magnetic oak wood and oak bark fast pyrolysis biochars. *Chem Eng J* 2014;236:513–28.
- [25] Pellera FM, Giannis A, Calderis D, Anastasiadou K, Stegmann R, Wang JY, Gidarakos E. Adsorption of Cu(II) ions from aqueous solutions on biochars prepared from agricultural by-products. *J Environ Manag* 2012;96(1):35–42.
- [26] Yao Y, Gao B, Zhang M, Inyang M, Zimmerman AR. Effect of biochar amendment on sorption and leaching of nitrate, ammonium, and phosphate in a sandy soil. *Chemosphere* 2012;89(11):1467–71.
- [27] Zhao L, Cao X, Mašek O, Zimmerman A. Heterogeneity of biochar properties as a function of feedstock sources and production temperatures. *J Hazard Mater* 2013;256:1–9.
- [28] Kloss S, Zehetner F, Dellantonio A, Hamid R, Ottner F, Liedtke V, Schwanninger M, Gerzabek MH, Soja G. Characterization of slow pyrolysis biochars: effects of feedstocks and pyrolysis temperature on biochar properties. *J Environ Quality* 2012;41(4):990–1000.
- [29] Brewer CE, Schmidt-Rohr K, Satrio JA, Brown RC. Characterization of biochar from fast pyrolysis and gasification systems. *Environ Prog Sustain Energy* 2009;28(3):386–96.
- [30] Huang K, Zhu H. Removal of Pb^{2+} from aqueous solution by adsorption on chemically modified muskmelon peel. *Environ Sci Pollut Res* 2013;20(7):4424–34.
- [31] Bhatnagar A, Kumar E, Minocha AK, Jeon BH, Song H, Seo YC. Removal of anionic dyes from water using *Citrus limonum* (lemon) peel: equilibrium studies and kinetic modeling. *Separ Sci Technol* 2009;44(2):316–34.
- [32] Langmuir I. The adsorption of gases on plane surfaces of glass, mica and platinum. *J Am Chem Soc* 1918;40(9):1361–403.
- [33] Freundlich HMF. Over the adsorption in solution. *J Phys Chem* 1906;57:385–471.
- [34] Dubinin MM, Radushkevich LV. Equation of the characteristic curve of activated charcoal. *Chem Zentr* 1947;1(1):875.
- [35] Hall KR, Eagleton LC, Acrivos A, Vermeulen T. Pore-and solid-diffusion kinetics in fixed-bed adsorption under constant-pattern conditions. *Ind Eng Chem Fundam* 1966;5(2):212–23.
- [36] Basci N, Kocadagistan E, Kocadagistan B. Biosorption of copper(II) from aqueous solutions by wheat shell. *Desalination* 2004;164(2):135–40.
- [37] Dahiya S, Tripathi RM, Hegde AG. Biosorption of heavy metals and radionuclide from aqueous solutions by pre-treated arca shell biomass. *J Hazard Mater* 2008;150(2):376–86.
- [38] SenthilKumar P, Ramalingam S, Sathyaselvabala V, Kirupha SD, Sivanesan S. Removal of copper(II) ions from aqueous solution by adsorption using cashew nut shell. *Desalination* 2011;266(1):63–71.
- [39] Grimm A, Zanzi R, Björnbom E, Cükierman AL. Comparison of different types of biomasses for copper biosorption. *Bioresour Technol* 2008;99(7):2559–65.
- [40] Pehlivan E, Altun T, Parlayici Ş. Modified barley straw as a potential biosorbent for removal of copper ions from aqueous solution. *Food chem* 2012;135(4):2229–34.
- [41] Hossain MA, Ngo HH, Guo WS, Setiadi T. Adsorption and desorption of copper (II) ions onto garden grass. *Bioresour Technol* 2012;121:386–95.
- [42] Cerino-Córdoba FJ, Diaz-Flores PE, García-Reyes RB, Soto-Regalado E, Gómez-González R, Garza-González MT, Bustamante-Alcántara E. Biosorption of Cu(II) and Pb(II) from aqueous solutions by chemically modified spent coffee grains. *Int J Environ Sci Technol* 2013;10(3):611–22.
- [43] Li YH, Ding J, Luan Z, Di Z, Zhu Y, Xu C, Wu D, Wei B. Competitive adsorption of Pb^{2+} , Cu^{2+} and Cd^{2+} ions from aqueous solutions by multiwalled carbon nanotubes. *Carbon* 2003;41(14):2787–92.
- [44] Li Y, Liu F, Xia B, Du Q, Zhang P, Wang D, Wang Z, Xia Y. Removal of copper from aqueous solution by carbon nanotube/calcium alginate composites. *J Hazard Mater* 2010;177(1):876–80.
- [45] Ge Y, Li Z, Xiao D, Xiong P, Ye N. Sulfonated multi-walled carbon nanotubes for the removal of copper(II) from aqueous solutions. *J Ind Eng Chem* 2014;20(4):1765–71.
- [46] Moradi O. The removal of ions by functionalized carbon nanotube: equilibrium, isotherms and thermodynamic studies. *Chem Biochem Eng Quart* 2011;25(2):229–40.
- [47] C. Srivastava V, Mall ID, Mishra IM. Modelling individual and competitive adsorption of cadmium(II) and zinc(II) metal ions from aqueous solution onto bagasse fly ash. *Sep Sci Technol* 2006;41(12):2685–710.

- [48] Srivastava VC, Mall ID, Mishra IM. Removal of cadmium(II) and zinc(II) metal ions from binary aqueous solution by rice husk ash. *Colloid Surfaces A: Physicochem Eng Asp* 2008;312(2):172–84.
- [49] Rao GP, Satyaveni S, Ramesh A, Seshaiah K, Murthy KS, Choudary NV. Sorption of cadmium and zinc from aqueous solutions by zeolite 4A, zeolite 13X and bentonite. *J Environ Manag* 2006;81(3):265–72.
- [50] Shukla SR, Pai RS. Adsorption of Cu(II), Ni(II) and Zn(II) on modified jute fibres. *Bioresour Technol* 2005;96(13):1430–8.
- [51] da Fonseca MG, de Oliveira MM, Arakaki LN. Removal of cadmium, zinc, manganese and chromium cations from aqueous solution by a clay mineral. *J Hazard Mater* 2006;137(1):288–92.
- [52] Kaya A, Ören AH. Adsorption of zinc from aqueous solutions to bentonite. *J Hazard Mater* 2005;125(1):183–9.
- [53] Guo XY, Liang S, Tian QH. Removal of heavy metal ions from aqueous solutions by adsorption using modified orange peel as adsorbent. In: Advanced Materials Research 2011 (Vol. 236, pp. 237–240). Trans Tech Publications.
- [54] Maheshwari U, Mathesan B, Gupta S. Efficient adsorbent for simultaneous removal of Cu(II), Zn(II) and Cr(VI); kinetic, thermodynamics and mass transfer mechanism. *Proc Safety Environ Protect* 2015;98:198–210.
- [55] Lagergren S. About the theory of so-called adsorption of soluble substances. *Kung Svenska Vetenskapsakademiens Handl* 1898;24(4):1–39.
- [56] Ho YS, McKay G. Pseudo-second order model for sorption processes. *Process Biochem* 1999;34:451–65.
- [57] Boyd GE, Adamson AW, Meyers LS. The exchange adsorption of ions from aqueous solutions by organic zeolites II. *J Am Chem Soc* 1947;69:2836–48.
- [58] Weber WJ, Morris JC. Kinetics of adsorption on carbon from solution. *J Sanit Eng Div Am Soc Civ Eng* 1963;89:31–60.